Feasibility of Displacement Monitoring using Low-cost GPS Receivers

Hongki Jo[1], Sung-Han Sim[2], Andrzej Tatkowski[3],
*B.F. Spencer, Jr.[4], and Mark E. Nelson[5]

[1), 3), 4)] *Department of Civil and Environmental Engineering*
University of Illinois at Urbana-Champaign, Urbana 61801, USA

[2)] *School of Urban and Environmental Engineering, UNIST, Ulsan 698-798, Korea*

[5)] *Department of Molecular & Integrative Physiology and*
the Beckman Institute for Advanced Science and Technology
University of Illinois at Urbana-Champaign, Urbana 61801, USA

[1)] *hjo4@illinois.edu,* [2)] *ssim@unist.ac.kr,* [3)] *tatkows1@illinois.edu*
[4)] *bfs@illinois.edu,* [5)] *m-nelson@illinois.edu*

ABSTRACT

Many of the available Structural Health Monitoring (SHM) approaches do not readily support displacement monitoring, nor do they work in concert with one another to take advantage of displacement based SHM for various long-period structures. While survey-quality Global Positioning System (GPS) technology offers the possibility of measuring such displacements with sub-centimeter precision, the associated cost is too high to allow for routine deployment. Low-cost GPS chips commonly found in mobile phones and automobile navigation equipment are attractive in terms of size, cost, and power consumption; however, the displacement accuracy of these GPS chips is on the order of several meters, which is insufficient for SHM applications. Inspired by sensory information processing strategies of weakly electric fish, this paper investigates the potential for using dense arrays of relatively low precision sensors to achieve high-precision displacement estimates. Results show that dynamic response resolution as low as 20-30 cm can be achieved and that the resolution scales with the sensor count.

1. INTRODUCTION

Recent catastrophic structural failures have focused public attention on the declining state of aging civil infrastructure and the necessity for Structural Health Monitoring (SHM). The

---

[1)] Graduate Student
[2)] Assistant Professor
[3)] Undergraduate Student
[4)] Nathan M. and Anne M. Newmark Endowed Chair in Civil Engineering
[5)] Professor

research community has turned to Wireless Smart Sensor Networks (WSSN) to develop approaches for continuously monitoring the health of essential infrastructure, both old and new. WSSNs offer many attractive features, such as ease of installation, wireless communication, on-board computation, battery-power, relatively low cost, and small size. Indeed, SHM using wireless smart sensor technology has emerged as a promising solution that will reduce inspection costs, optimize repairs, and ensure public safety as building and bridge structures get higher, longer, and more complex. Recent successful implementations of WSSN for full-scale SHM systems have demonstrated the practical use of the technology (Jang et al. 2010; Cho et al. 2010; Kurata et al. 2010).

However, most current SHM approaches using WSSN, even for traditional wired systems, rarely support displacement monitoring, primarily due to the difficulty in measuring absolute displacements. Many of advantages of displacement based SHM for long-period structures such as high-rise buildings and cable-supported bridges are left untapped.

Global Positioning System (GPS) technologies are able to provide absolute displacement measurements. A state-of-the-art Real-Time Kinematic (RTK) technique with dual-frequency GPS receivers that can use L1/L2 carrier phases allows for sub-centimeter accuracy. However, this kind of dual-frequency GPS sensor is quite high in cost, making it unsuitable for dense deployments which are critical for damage detection. On the other hand, C/A code-based single-frequency low-cost GPS receivers generally used for navigation purposes are potentially suitable for dense deployments using smart sensors due to their small size, low cost, and relatively low power consumption. However, the resolution of these low-cost GPS sensors is quite low (on the order of meters); therefore, their application to SHM has not yet been reported.

Mimicking biological signal processing strategies has tremendous potential for improving the quality of information obtained in WSSN applications. Inspiration for this work comes from weakly electric fish found in South America and Africa (see Fig. 1). These fish generate electrical fields using a specialized electric organ located in the tail region of the fish (black bar in the right of Fig. 1) to actively probe their environment (Nelson 2011). These fish emit millivolt-level electrical discharges and detect microvolt-level voltage perturbations arising from nearby objects in the water. This phenomenon is called as electrolocation and is analogous to echolocation abilities found in bats and dolphins (see the right of Fig. 1). The body of a weakly electric fish is covered with around 15,000 electroreceptors. Each individual electroreceptor, however, is a relatively low-resolution sensor and does not provide reliable event detection. To compensate for this, the nervous system of the electric fish creates arrays of virtual sensors with the desired resolution and sensitivity by pooling information from multiple low-resolution skin sensors. This approach allows the fish to detect and localize targets in 3D space and assess target characteristics such as size, shape and electrical impedance. This suggests the possibility of designing a WSSN that achieves high-precision displacement measurements using a dense array of low-cost GPS sensors.

This study investigates the potential for using low-cost GPS sensors to obtain displacement measurements suitable for monitoring large civil infrastructure. First, the accuracy of low-cost GPS modules is assessed through various static and dynamic tests and through analyzing the correlation characteristics of the noise in the GPS signals. Analytical studies are also considered to assess the potential of using dense arrays of such GPS sensors.

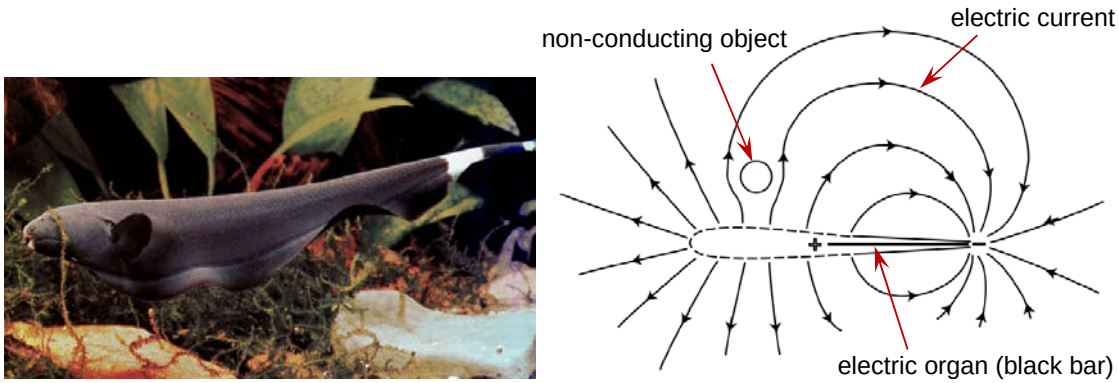

Fig. 1. Weakly electric fish (left) and principal of electrolocation (right) (Nelson 2011)

2. C/A CODE BASED LOW-COST GPS RECEIVERS

2.1 GPS signals and frequencies

A GPS satellite broadcasts a navigation message at a rate of 50 bps. Each message contains the satellite clock, satellite location, and status of the satellite. The messages are encoded using Code Division Multiple Access (CDMA), allowing messages from individual satellites to be distinguished from one another based on unique encodings for each satellite. Two distinct types of CDMA encodings are used: coarse/acquisition (C/A) code, which is freely available to the public, and the precise (P) code, which is usually reserved for military applications. All satellites broadcast at the same two frequencies: one at 1575.42MHz (10.23MHz × 154), called the L1 carrier, and second at 1227.6MHz (10.23MHz × 120), called the L2 carrier. The C/A code is transmitted on the L1 carrier at 1.023MHz, and the P code is transmitted on the both L1 and L2 carrier at 10.23MHz, but 90° out of phase with C/A code on the L1. Fig. 2 shows the modulation scheme of GPS signals.

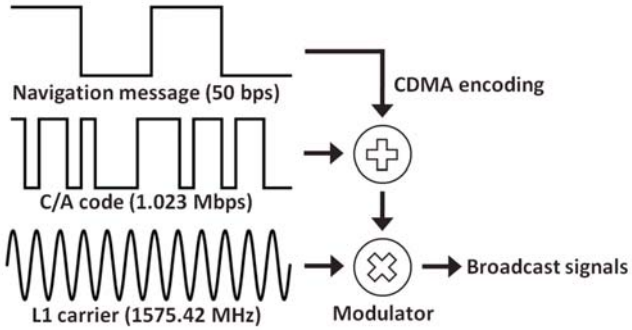

Fig. 2. GPS signal modulation scheme
(from http://da.wikipedia.org/wiki/Global_Positioning_System)

2.2 GPS receiver types

There are two different types of GPS receivers in terms of frequency usage; one is the single-frequency (L1) C/A code based GPS receiver, which is usually used for navigation purposes, and the other one is the dual-frequency (L1 & L2) carrier-phase based GPS receiver. The accuracy of receivers is generally a function of the ability of the receivers' electronics to accurately compare the signal sent from the satellite and an internally generated copy of the same signal within the receiver. Using the time delay between the GPS signal and the receiver's signal, the distance from the satellite can be calculated. Considering the wavelengths of the C/A code (3×10^8 m/s / 1.023×10^6 Hz = 293.3 m) and the L1 carrier (3×10^8 m/s / 1575.42×10^6 Hz = 0.190 m), even a 1% alignment error, for instance, can cause 2.933 m of error for single-frequency GPS and 1.9 mm of error for dual-frequency GPS. Assuming the same alignment error, the accuracy of the dual-frequency GPS receiver that uses both the L1 and L2 carriers with frequencies 1575.42MHz and 1227.6MHz will be about 1500 times better than the single-frequency GPS receiver using C/A code with a frequency of 1.023MHz. Of course, effects other than alignment error can introduce additional errors. The overall accuracy of GPS receivers is at the meters level for single-frequency GPS receivers and at the centimeters level for dual-frequency GPS receivers.

Dual-frequency GPS systems have been widely used for displacement monitoring purposes because of their high accuracy. The Real Time Kinematic (RTK) technique, which provides real-time correction using a Differential GPS (DGPS) method, enables even millimeter level accuracy. However, due to high cost (typically tens of thousands of dollars per a unit), only a small number of units can be deployed on a structure.

C/A code based GPS receivers are cheap, small, and consume little power, which offers the potential for deploying a dense array of such sensors. However, the meters-level accuracy is still insufficient for SHM applications. As a result, neither the use nor the feasibility of using low-cost C/A code based GPS receivers for SHM applications has been reported to date.

Fig. 3. Leica GMX902 dual-frequency GPS receiver (left) and AX1202 antenna (right): 0.2mm RMS accuracy, 2.4W power consumption, and up to 20Hz sampling rate (Leica 2005).

In this study, instead of using a single GPS receiver, a dense array of the C/A code based low-cost GPS receivers is explored for SHM applications, mimicking the weakly electric fish's ability to construct virtual high-sensitivity sensor nodes using many low-resolution skin sensors.

2.4 MT3329 GPS chipset (C/A code based single-frequency GPS module)

Recently, GlobalTop has released a new high-sensitivity and low-power GPS module (Gms-u1LP, see Fig. 4). It uses the MediaTek MT3329 GPS chipset (L1 frequency, C/A code, 66 channels), consumes only 24mA at 3.3V, contains an integrated ceramic antenna, features -162dBm of sensitivity, has 3.0m RMS of position accuracy, and is relatively small in size (16×16×6mm). Also, it supports sampling rates up to 10Hz and costs only about $20 per unit. Moreover, it comes with customizable software, although some core algorithms cannot be accessed. These characteristics offer the potential for implementation in a WSSN.

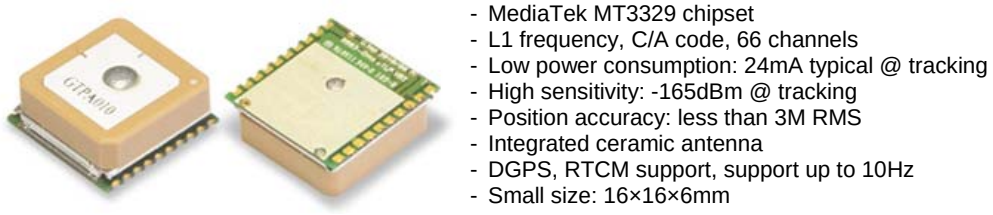

Fig. 4. Gms-u1LP single-frequency GPS module with integrated antenna (GlobalTop, 2010)

3. PRELIMINARY GPS TESTING

3.1 Experiment set-up

To assess the feasibility of low-cost GPS receivers for SHM applications, the achievable accuracy and limitations of the GPS need to be identified in both static and dynamic conditions. For this preliminary investigation, four GlobalTop Gms-u1LP GPS modules with the integrated ceramic antennas were used. The four GPS receivers were placed together on a small wooden plate, and FTDI cables were used to convert UART (TTL) serial data from the GPS receivers to USB signals, which were then transmitted to a laptop computer. The GPS data, in NMEA 0183 format, is recorded through the HyperTerminal program included in Microsoft Windows XP. Static and dynamic tests were performed on the roof of the Newmark Civil Engineering Laboratory (NCEL) building located in the University of Illinois at Urbana-Champaign campus. Even though there were several small steel chimneys, about 30 centimeters in diameter and 2 meters in height, the roof provided a quite open field environment, free from other buildings that may obstruct the view of low elevation satellites.

3.2 Static tests

Static calibration tests were carried out to assess the variation in the static measurements over time and to assess the possibility of using the DGPS concept with low-cost single frequency GPS receivers. Additionally, these tests were executed to quantify the background noise characteristics in actual GPS measurements on a structure. These four GPS receivers were placed at a fixed location on the roof of the NCEL building, and four consecutive days of data, from March 1st through 4th, 2011, were measured at a 1 Hz sampling rate. The first three days were sunny with no clouds, and the last day was rainy with weak thunderstorm conditions in the

Champaign-Urbana area.

Because the full 24 hours day measurements are too long to be shown clearly, only12 hours of data, from midnight to noon, are plotted in Fig. 5; the left column compares measurements from a single GPS receiver across 4 days and the right column compares readings from four GPS receivers on a single day.

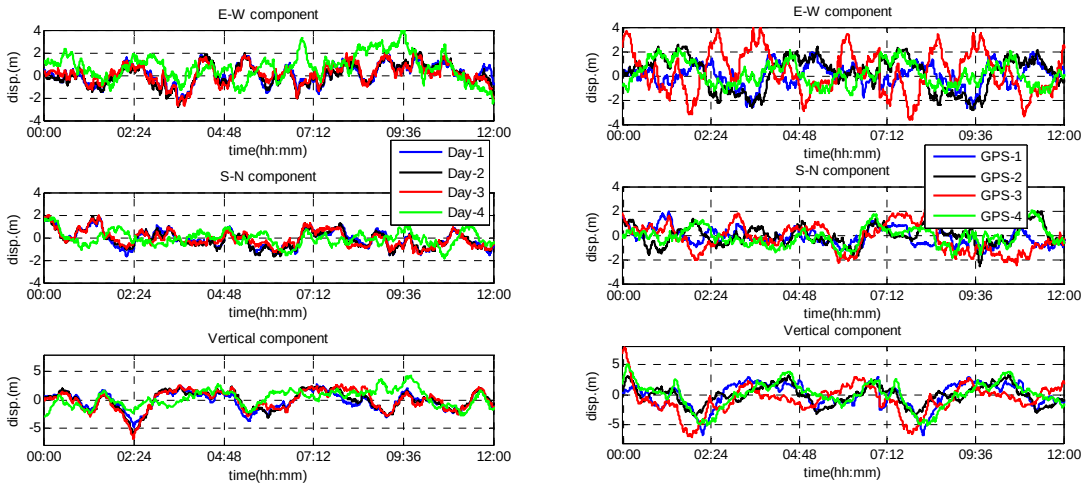

Fig. 5. Static measurement comparisons: GPS-1 data for 4 days (left), GPS 1~4 data for 3rd day (right)

As shown in the left column of Fig. 5, very strong correlation is found between the static data for the first three days for GPS-1, while the data for the fourth day deviated significantly from the previous three. Considering the orbital period of GPS satellites is 12 hours and the multipath-distortion would be repeated every orbital period, the correlated noises can be predicted and subtracted from the actual structural measurements in the future. However, the elimination of the repeated noise seems to be valid only for days with clear skies; the static data measured in the rainy day (Day 4) was quite different from the other three days' data.

To utilize DGPS technique, which can be realized with a correction signal from a reference GPS station placed at a fixed location, the reference and mobile GPS modules need to be assumed to have same amount of static noise. However, even on a sunny day, the static noise among the four different GPS modules did not show strong correlation (see Fig. 5, right column). Thus, the DGPS concept with low-cost GPS sensors may not be useful in practice.

Fig. 6 shows the correlation between the data from the first two days with clear skies in E/W, N/S, and vertical directions. The root mean square (RMS) value changes of the static measurements for all days are plotted in Fig. 7. The RMS errors for the first three sunny days' data were about 1m and slightly increased for the rainy day measurement in the horizontal directions. In comparison with other GPS modules, GPS-3 showed larger RMS errors in the E/W and vertical directions. However, these errors are still less than the position accuracy of 3m RMS specified in the datasheet of the GlobalTop Gms-u1LP module.

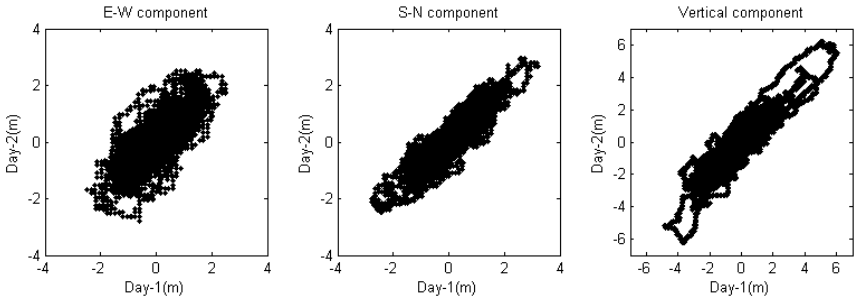

Fig. 6. Correlation between days: East/West component (left), South/North (middle), and vertical component (right)

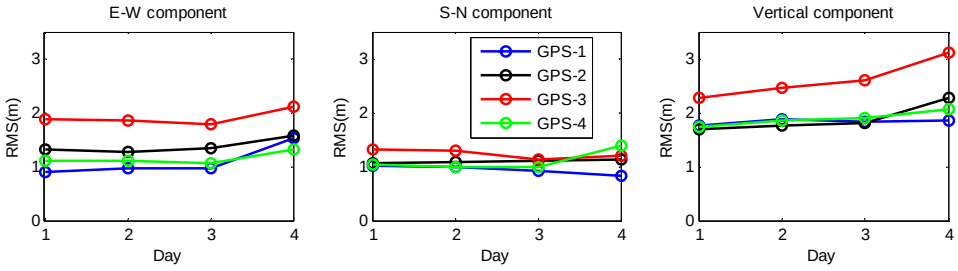

Fig. 7. RMS value changes of static measurement over all days: E/W component (left), S/N (middle), and vertical component (right)

3.3 Dynamic tests

To check the applicability of low-cost GPS sensors to dynamic displacement measurements, calibration tests were performed. A horizontal rotor blade was constructed for the preliminary dynamic tests (see Fig. 8). A wooden plank, 2.0m long and 0.3m wide, was fixed on top of a DC gear motor having 1/8 HP and a maximum rotational speed of 33 RPM. When assembled, the device equivalently has two 1.0m long blades extending in opposite directions from the central motor. The four GlobalTop Gms-u1LP GPS sensors were placed together at given locations on the blades, and a laptop was used to power and receive data from the GPS sensors. The laptop was powered using a rechargeable car battery, and both the battery and laptop were placed on the center of the wooden plate. Varied rotational speeds were tested to quantify the range of frequencies and amplitudes that could be successfully tracked using the low-cost single-frequency GPS sensors. A 5 Hz sampling rate was used for the dynamic tests.

Fig. 9 shows the time histories of 30 minutes of measurements in a circular motion at a 1.0m radial distance with a 2.3 second rotational period for all four GPS modules. The simultaneous E/W and N/S components shown in the left diagram of Fig. 9 seem not to provide any appearance of circular motion; they even seem to be contaminated with drifting noises of over ±5m. However, clear sinusoidal waves were observed in the each directional component of the 1-minute detail plotted on the right in Fig. 9. They measured the dynamic movement well; nevertheless some low-frequency drift errors are present.

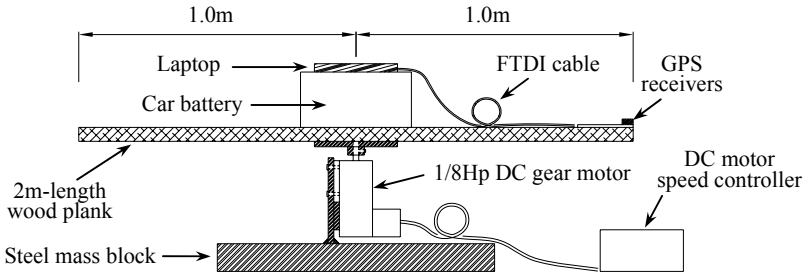

Fig. 8. Rotor blade for GPS dynamic testing

Fig. 9 shows the time histories of 30 minutes of measurements in a circular motion at a 1.0m radial distance with a 2.3 second rotational period for all four GPS modules. The simultaneous E/W and N/S components shown in the left diagram of Fig. 9 seem not to provide any appearance of circular motion; they even seem to be contaminated with drifting noises of over ±5m. However, clear sinusoidal waves were observed in the each directional component of the 1-minute detail plotted on the right in Fig. 9. They measured the dynamic movement well; nevertheless some low-frequency drift errors are present.

The power spectral densities (PSDs) clearly showed the frequency contents of the time histories in Fig. 10. The frequency of 0.43Hz corresponding the rotor's rotational speed was shown in both E/W and N/S directions. However, unexpected additional peaks were observed around 0.86Hz and 1.29Hz. These additional frequencies may be attributed to nonlinearities associated with quantization error of the GPS measurements, which can cause periodical round-off error in circular movements; the resolution of the latitude and longitude measurements expressed in NMEA format (dddmm.mmmm) corresponds to about 0.142m.

The PSDs also show the noise characteristics of the GPS measurements, which look similar to a $1/f$-shaped noise spectrum; above the 1-Hz region, the noise is more white in nature and the level significantly increases towards the DC area. These $1/f$-like noises may cause the low-frequency drifting error seen in the time histories of the right side of Fig. 9. In general, displacement measurements have been known to be more accurate in low-frequency area than other measurements, such as velocity or acceleration. However, this view may not be valid for displacement measurement using the single-frequency low-cost GPS receivers; the more dominant noises exist in the lower frequency region.

Another observation was made in the time and frequency domain. As shown in the right of Fig. 9, the drift component of the signal seems to be quite random. The PSD diagrams support this observation. The PSD of the average of the four GPS measurements showed lower noise levels (thick black lines in Fig. 10); averaging the four time histories resulted in a 6dB decrease in the noise level over the entire frequency range. The cross power spectral density (CPSD) of two signals also provides an indication of the correlation of the signal drift. For example, the cross PSD of GPS-2 and GPS-4 showed lower noise levels than auto PSD of each GPS measurement (see Fig. 11).

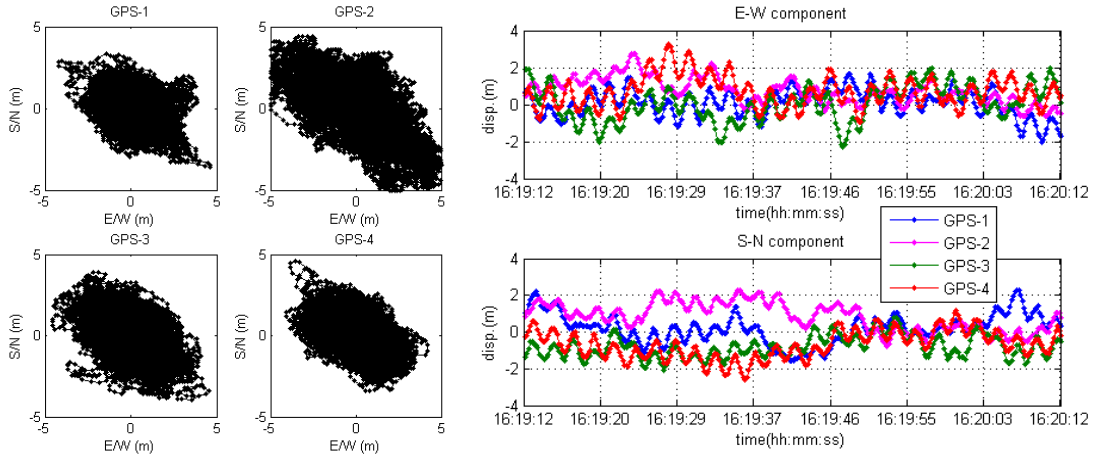

Fig. 9. Dynamic measurements (1.0m radius and 2.3sec period): 30 minutes data in both directions (left) and each directional component of 1-minute data (right)

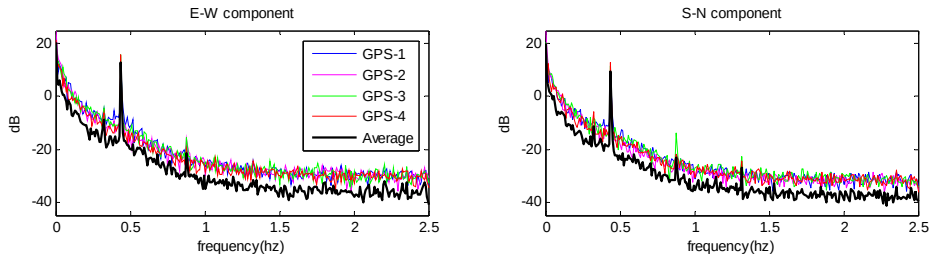

Fig. 10. PSDs of the GPS measurements in E-W direction (left) and S-N direction (right): 1.0 m radius and 2.3 sec period

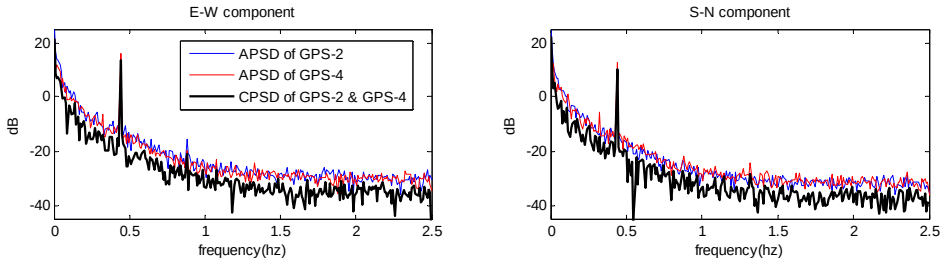

Fig. 11. PSDs and CPSD of the GPS-2 & GPS-4 measurements in E-W direction (left) and S-N direction (right): 1.0 m radius and 2.3 sec period

3.4 GPS signal simulation

Based on the previous observation made from Fig. 10-11, 1/*f*-like noise is used to better understand the characteristics of the low-cost GPS modules and simulate their performance.

Many researchers have previously tried to identify these noise characteristics and simulate them, considering numerous GPS noise sources (Genrich and Bock 2006, Amiri-Simkooei et al. 2007; Borsa 2007). In this study, however, only the statistical characteristics of the noise are of interest; consideration of specific effects of individual noise sources is not sought.

Passing white noise through a filter can easily produce the 1/*f*-like shaped noise. For this study, the $1/f^{\alpha}$ power law noise model is used (Kasdin 1995). In a discrete representation, the resulting spectrum has the form of

$$S_d(f) = Q_d \Delta t^{1-\alpha} / (2\pi f)^{\alpha}, \tag{1}$$

where Q_d is the variance of the input white noise. The transfer function of the $1/f^{\alpha}$ AR filter has the form of

$$H(z) = \frac{1}{a_0 + a_1 z^{-1} + a_2 z^{-2} + a_3 z^{-3} \cdots}, \tag{2}$$

where $z = e^{j2\pi f \Delta t}$ and the filter coefficients for this are

$$\begin{aligned} a_0 &= 1 \\ a_k &= \left(k - 1 - \frac{\alpha}{2}\right) \cdot \frac{a_{k-1}}{k}, \quad k = 1, 2, 3 \ldots \end{aligned} \tag{3}$$

A sinusoidal wave of 0.43Hz was generated and then combined with the $1/f^{\alpha}$ shaped white noise to simulate the GPS measurement. A round-off error of 0.142m, corresponding to the previously mentioned quantization error, is introduced to see if additional frequency peaks appear in the PSD diagram. Fig. 12 shows the time histories and PSDs of the simulated GPS measurements. In total, one-hundred GPS measurements are simulated; one of the typical time histories and the simulation procedure are shown on the left of Fig. 12, and their PSDs on the right.

As shown in Fig. 12, the spectrum of the simulated noise has the mentioned 1/*f*-like form (right). The time history shows a drift noise, mainly due to more energy in the low-frequency area (left), as seen in the actual measurements in Fig. 10-11. The round-off error introduced in the sinusoidal motions gives rise to extra peaks in the PSD, as expected (see the right of Fig. 12); without the round-off error, there were no additional frequency peaks. Also, the noise reduction effects were observed when the simulated GPS signals were averaged (see the right bottom of Fig. 12). Because the simulated GPS noises are based on uncorrelated white noise, the uncorrelated noises should be averaged out during the averaging process. Through the averaging process of four simulated GPS signals, around a 6dB noise reduction effect was observed, which is similar to the phenomenon seen in actual data (see Fig. 10). The averaging process of one-hundred signals created additional noise reduction, in which the PSD of the averaged signal approaches the PSD of the sinusoidal signal (purple line in the right of Fig. 12), indicating the potential of utilizing a dense array of low-cost GPS sensors.

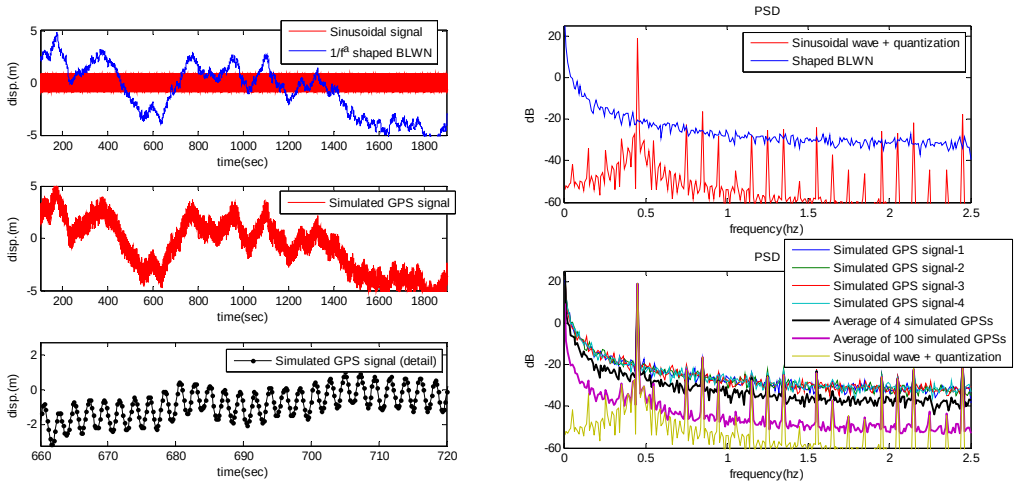

Fig. 12. Time histories (left) and PSDs (right) of simulated GPS measurements

3.5 Displacement amplitude change over time

In the dynamic tests, the radius of the circular movements was 1.0m. However, long-term records spanning 30 minutes showed lower amplitudes than the expected value. To better identify the characteristics of the measured GPS signals without noise, the time history data shown in Fig. 9 were band-pass filtered. As shown in Fig. 13, the band-pass filtered signals showed an amplitude which was about half of the actual value; moreover, the amplitudes changed both with time and between different GPS units. The RMS values of the ratio between the GPS measurements and the expected value were 0.43 for the E/W direction and 0.39 for the N/S direction for the average of four GPS modules; they were less than 1 and had a different value in each of the directions.

The amplitude variation phenomenon also has been reported in a dual-frequency GPS testing (Casciati & Fuggini 2009). The measured displacement amplitudes using dual-frequency RTK GPS receivers (Leica GMX902) fluctuated over time; the RMS values of the ratio between the GPS measurement and the expected value differ (RMS=0.85~1.2) between different frequencies and different amplitudes, although the errors were the order of sub-centimeters. For the low-cost GPS sensors, the amplitude variation phenomenon seems more severe. More testing results with different amplitude and frequency combinations are discussed in the following section.

One of the main reasons for the directional difference of the RMS values may be the uneven GPS satellite distribution across the sky in mid-latitude areas (Meng et al. 2004). Due to the 55° inclination of satellite orbits, no observation is possible in the northern sky quadrant. Fig. 14 shows the satellite sky view on the roof of the NCEL building at Illinois, and also shows the large hole having no satellite traces in the northern sky area. Such a satellite sky distribution should result in worse accuracy in the North/South direction than in the East/West direction, which was confirmed by the data measured in this study. For this reason, in the following dynamic test, only the E-W component of the measurement will be considered.

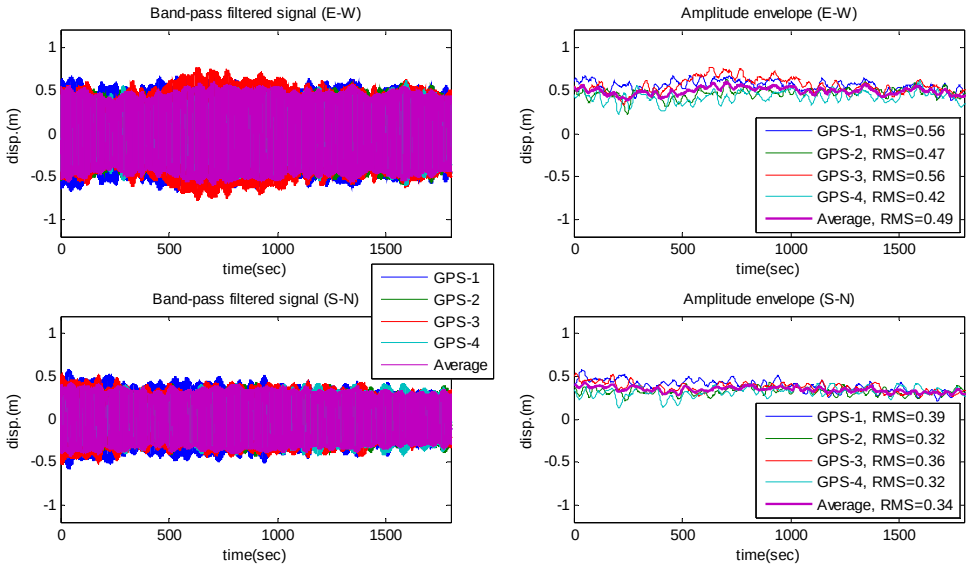

Fig. 13. Bandpass filtered time histories (left) and amplitude envelope (right)

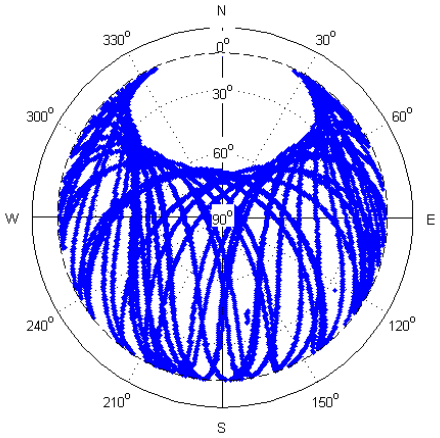

Fig. 14. Satellite sky view on the NCEL building at Illinois on May 15th, 2011

4. PARAMETRIC DYNAMIC GPS TESTING

To evaluate the performance of the low-cost GPS receivers at different frequencies and displacement amplitudes, parametric dynamic testing was carried out for various combinations of frequencies and amplitudes by changing the rotational speed of the rotor blade and moving the GPS locations along the wooden rotor blade. In this test, six different amplitudes, 0.25m, 0.5m, 0.75m, 1m, 1.5m and 2m, and five different rotational frequencies, 0.098Hz, 0.195Hz, 0.215Hz, 0.461Hz, and 0.68Hz were used, while the other sensing parameters remained

unchanged from the previous dynamic tests. The wooden rotor blade was extended to have a 2-m length from the center of rotation.

Because the generated data is too extensive to include in this paper, only one of typical sets of measurements is plotted in Fig. 15~17 (the 0.215Hz rotational frequency test). Fig. 16 shows the time histories of measured displacements for the six different amplitudes from the four Gms-u1LP GPS sensors. Fig. 16 shows the PSDs of the measurements, and Fig. 17 shows the band-pass filtered time histories. Although some GPS sensors sometimes broke away from the behavior of the others, the average of the four GPSs showed consistent performance over time and for the various testing cases.

As the rotational radius of the GPS sensors changed from 0.25m to 2m, obvious differences in the measured displacement amplitudes were observed (see Fig. 15). This observation is even clearer in Fig. 17, which shows the band-pass filtered signal; the larger the radius of rotation was used, the larger the displacement amplitudes were measured.

The PSDs for different amplitudes clearly show the corresponding rotational frequency peak at 0.215Hz, even for the 0.25m amplitude case (see Fig. 16). The frequency peak magnitudes for different amplitude cases are different. In the frequency domain, the low-cost GPS sensors showed satisfactory performance. However, as the amplitude becomes smaller, it becomes more contaminated and affected by the low-frequency drift noises. Also, the additional peaks in the PSDs, which should not be there, appeared as expected. The periodical round-off error in the cyclic rotational movement may be the reason, as simulated in Fig. 12.

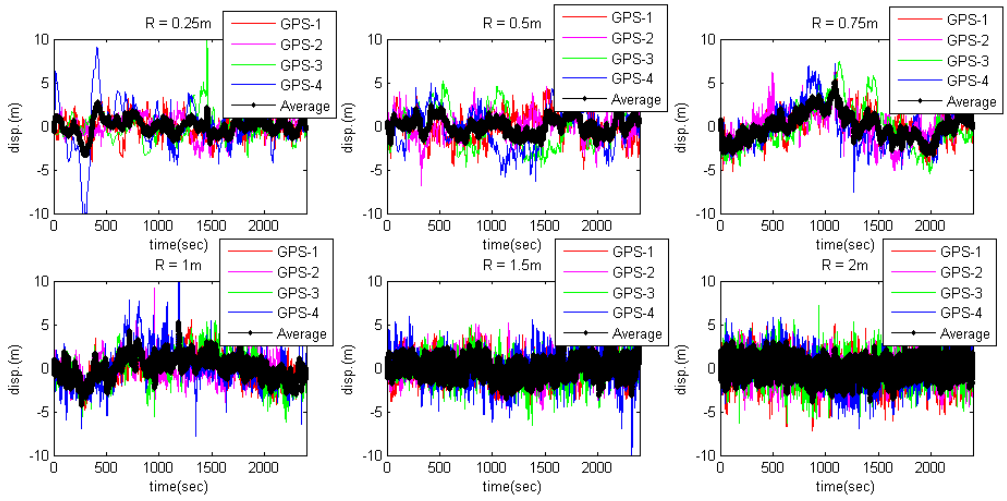

Fig. 15. GPS displacement time histories for six different amplitudes at 0.215Hz

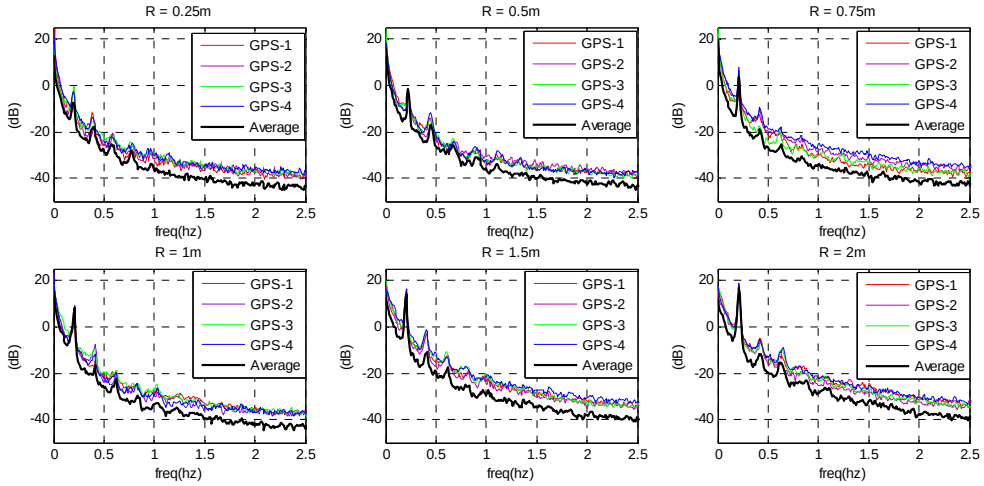

Fig. 16. GPS displacement PSDs for six different amplitudes at 0.215Hz

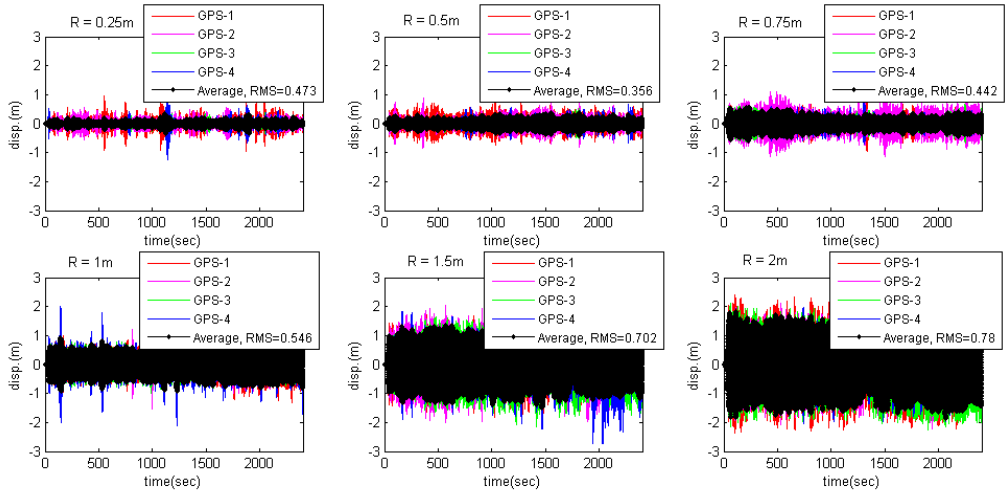

Fig. 17. Band-pass filtered GPS time histories for six different amplitudes at 0.215Hz

Fig. 17 shows the RMS values of the ratio between the measured amplitudes and the expected amplitudes at different rotational frequencies and different displacement amplitudes. Even though further validation is required to draw a conclusion, a trend can be confirmed by similar behaviors for tests with different cases. As shown in Fig. 18, it is observed that as the rotation amplitude increases, the closer the RMS value is to 1 (left), and as the rotational frequency decreases, the closer the RMS value is to 1 (right).

For the lowest rotational speed of 0.098Hz, the measurements were contaminated with much low-frequency noise. Though the RMS values for the 0.098Hz case, except R=0.25m case,

were generally close to 1 (green line in the left of Fig. 18); however, it was because the noise floor in low-frequency range is too high (1/*f* shape). Even for the 1-m amplitude case data was overwhelmed by the noise (see Fig. 19, middle). The other higher frequency cases, on the other hand, showed consistently reasonable results (Fig. 19, left); the larger amplitude cases yielded more accurate RMS values.

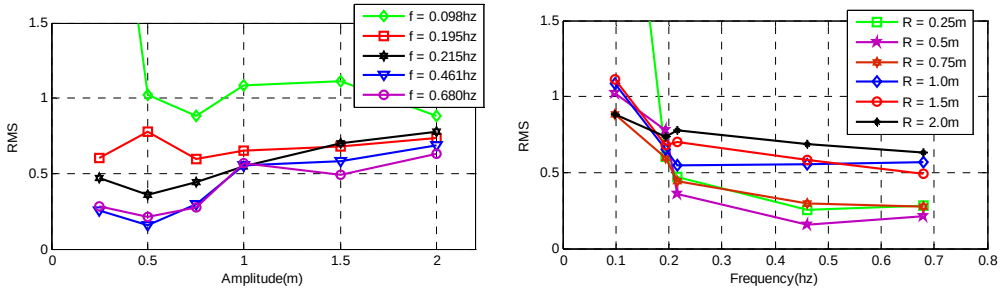

Fig. 18. RMS value changes of measured displacement amplitude in different amplitudes (left) and different frequencies (right)

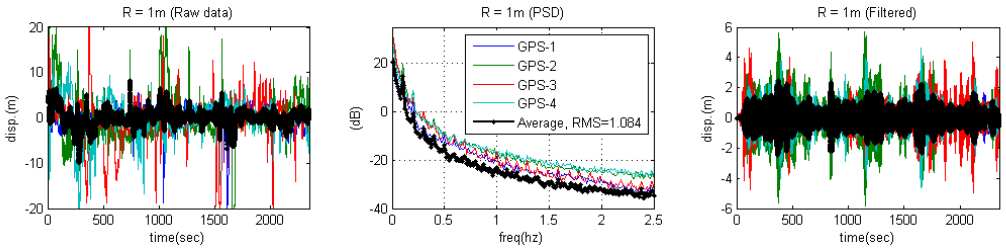

Fig. 19. GPS measurement with 1m amplitude and at 0.098Hz frequency: time histories (left), PSD (middle), and band-pass filtered time histories (right)

As for the effect of rotational frequencies on the performance of the GPS receivers, (Fig. 18, right), the data showed that better accuracies were present at lower frequencies; the GPS modules better caught the rotational movements at lower speeds. According to the manufacturer of the Gms-u1LP GPS receivers, GlobalTop, this kind of single-frequency GPS contains a function that filters erratic movements in order to obtain better tracking, which is usually used to optimize the receivers for car or pedestrian navigation purposes. Because the GPS sensors on the rotational blade recognize a change in direction each time the position is sampled, as the rotational speed increases, the directional angle change also increases; this could be recognized as the erratic change by the GPS receivers, so long as the angle change is larger than a certain threshold. Of course, this sort of filtering technique will undoubtedly lead to degradation in positioning accuracy in such rotational movements; however, it could be helpful with straight or smooth movements.

CONCLUSIONS

The feasibility of low-cost single frequency GPS receivers for SHM applications and the bio-inspired displacement strategy using a dense array of the GPS sensors has been investigated in this paper. To identify the performance of the low-cost GPS receivers, diverse static and dynamic experimental tests have been performed. Also, simulated GPS data has been used and compared with real measurements in order to Fig. out the GPS noise characteristics.

In the static tests, periodic static noises in individual GPS modules over several days were observed, which could be predicted and subtracted from measurements, similar to how sensory expectation is suppressed in the nervous system of the electric fish. However, long-term tests using multiple GPS sensors showed that the repeatability of the static data is affected by weather conditions and non-uniform hardware quality of each sensor.

Through the dynamic tests using horizontal rotor system, low-frequency drift was observed in the GPS measurements, which had a $1/f$ spectrum. Similar to how the electric fish averages signals from many low-resolution skin sensors to extract necessary information, averaging multiple GPS measurements reduced the noise level, consequently making more apparent frequency peaks in PSD; the noise had low correlation, so averaging process could reduce the noise levels, and the cross PSD of two different GPS measurements and the simulated GPS data confirmed that GPS noises have low correlation.

The ability of the GPS receivers to capture dynamic displacement responses was quite satisfactory. Even at 0.25m amplitude, oscillations were captured and appeared clearly in frequency domain. However, amplitude fluctuations and loss were observed over time. The dynamic tests with various combinations of amplitudes and frequencies showed that the precision depended on the amplitude and frequency of the signal. Furthermore, the displacement measurements at very low frequency ranges were very noisy due to $1/f$-like noise. Also, poor distribution of the GPS satellites in northern sky diminished positioning accuracy in the North/South measurement direction.

In summary, the possibilities and limitations of the low-cost GPS sensors for SHM applications were explored in this study. The GPS measurements provided quite satisfactory information in the frequency domain, which still can be useful for long-period and large deformation structures such as cable-suspended bridges, even though the hardware and software capabilities of the low-cost GPSs are not yet advanced enough for broader SHM applications.

REFERENCES

Amiri-Simkooei, A.R., Tiberus, C.C.J.M, and Teunissen, P.J.G. (2007), "Assessment of noise in GPS coordinate time seriesL methodology and results," *Journal of Geophysical Research*, Vol. 112(B07413). Doi 10.1029/2006JB004913.

Borsa, A.A. and Minster, J.B. (2007), "Modeling long-period noise in kinematic GPS applications," *Journal of Geodesy*, Vol. 81, 157-170.

Casciati, F. and Fuggini, C. (2009), "Engineering vibration monitoring by GPS: long duration records," *Earthquake Engineering and Engineering Vibration*, Vol. 8(3), 459-467.

Cho, S., Jo, H., Jang, S.A., Park, J., Jung, H.J., Yun, C.B., Spencer, Jr., B.F., and Seo, J. (2010), "Structural health monitoring of a cable-stayed bridge using smart sensor technology: data analyses," *Smart Structures and Systems*, Vol. 6(5-6), 461-480.

Genrich, J.F., Bock, Y. (2006), “Instantaneous geodetic positioning with 10-50Hz GPS measurements: noise characteristics and implications for monitoring networks,” *Journal of Geophysical Research*, Vol. 111(B03403). Doi 10.1029/2005Jb003617.

GlobalTop Technology Inc (2010), “Gms-u1LP GPS module data sheet”, Tainan, Taiwan, http://www.gtop-tech.com.

Jang, S.A., Jo, H., Cho, S., Mechitov, K.A., Rice, J.A., Sim, S.H., Jung, H.J., Yun, C.B., Spencer, Jr., B.F., and Agha, G. (2010), “Structural health monitoring of a cable-stayed bridge using smart sensor technology: deployment and evaluation,” *Smart Structures and Systems*, Vol. 6(5-6), 439-459.

Kasdin, N.J. (2005), “Discrete simulation of colored noises and stochastic process and $1/f^{\alpha}$ power law noise generation,” *Proc. of the IEEE*, Vol. 83(5), 802-827.

Kurata, M., Kim, J., Zhang, Y., Lynch, J.P., Linden, G.W., Jacob, V., Thometz, E., Hipley, P. and Sheng, L.H. (2010), "Long-term assessment of an autonomous wireless structural health monitoring system at the New Carquinez Suspension Birdge", *Proc. of SPIE,* San Diego.

Leica Geosystems AG (2005), “GMX 902 User manual”, Heerbrugg, Switzerland.

Meng, X., Roberts, G.W., Dodson, A.H., Cosser, E., Barnes, J. and Rizos, C. (2004), “Impact of GPS satellite and pseudolite geometry on structural deformation monitoring: analytical and empirical studies,” *Journal of Geodesy*, Vol. 77, 809-822.

Nelson, M.E. (2011), "Biological smart sensing strategies in weakly electric fish,” *Smart Structures and Systems,* Vol. 8(1).

Yi, TingHua, Li, HongNan and Gu, Ming (2010), "Recent research and applications of GPS based technology for bridge health monitoring," *Science China Tech. Sci.,* Vol. 53(10), 2597-2610.